CHALMERS
UNIVERSITY OF TECHNOLOGY

Novel suspension route to incorporate graphene nano-platelets in HVAF-sprayed Cr3C2-NiCr coatings for superior wear performance

Available online at www.sciencedirect.com

jmr&t Journal of Materials Research and Technology

journal homepage: www.elsevier.com/locate/jmrt

Original Article

Novel suspension route to incorporate graphene nano-platelets in HVAF-sprayed Cr_3C_2–NiCr coatings for superior wear performance

Satyapal Mahade [a,*], *Antonio Mulone* [b], *Stefan Björklund* [a], *Uta Klement* [b], *Shrikant Joshi* [a]

[a] *Department of Engineering Science, University West, Trollhättan, Sweden*
[b] *Department of Industrial and Materials Science, Chalmers University of Technology, Gothenburg, Sweden*

ARTICLE INFO

Article history:
Received 25 January 2021
Accepted 28 April 2021
Available online 7 May 2021

Keywords:
Cr_3C_2–NiCr
Graphene nano-platelets (GNP)
High velocity air fuel (HVAF)
Powder- suspension hybrid
Sliding wear

ABSTRACT

Graphene nano platelets (GNP) have several attractive properties, including excellent lubricity that can be used to develop wear-resistant coatings. Thermally sprayed chromium carbide–nickel chromium (Cr_3C_2–NiCr) coatings are widely employed to impart wear resistance to engineering components. This work attempts to improve the wear resistance of high velocity air fuel (HVAF) sprayed Cr_3C_2–NiCr coatings by incorporating GNP using a hybrid approach in which Cr_3C_2–NiCr (powder) and GNP (suspension) are co-axially injected. Two different powder-to-suspension delivery ratios were employed in this study that utilizes a liquid feedstock in tandem with a HVAF system. Furthermore, for comparison, a pure (without graphene) Cr_3C_2–NiCr reference coating was deposited by the HVAF process using identical spray parameters. The as-sprayed coatings were characterized for their microstructure and phase constitution by SEM/EDS and X-Ray Diffraction. Mechanical properties such as hardness and fracture toughness were evaluated using micro-indentation technique. The hybrid coatings were subjected to dry sliding wear tests and wear performance was compared with reference Cr_3C_2–NiCr. The GNP incorporated hybrid coatings exhibited lower CoF and lower wear rates than the reference Cr_3C_2–NiCr coating. Post wear SEM/EDS analysis revealed different wear mechanisms predominant in the investigated coatings. Utilizing the above as a case study, this work provides key insights into a new approach to produce GNP incorporated coatings for mitigating wear.

1. Introduction

Wear contributes to inferior performance of engineering components and often results in economic losses due to premature component failure and unscheduled maintenance related halts. Coatings of various materials such as ceramics, metals, cermets etc., are used to mitigate wear [1,2]. Material choice for combating wear typically depends on the performance requirements for the intended application. Among the existing cermet coating compositions, WC-Co coatings are preferred due to their exceptional wear performance [3–6].

* Corresponding author.
E-mail address: satyapal.mahade@hv.se (S. Mahade).
https://doi.org/10.1016/j.jmrt.2021.04.096

One drawback of WC-Co coatings is their toxic nature, as 'Co' (Cobalt) is known to be carcinogenic, which exposes the operator to potential health related hazards [7,8]. Consequently, increasingly stringent industry demands regarding safety are gradually forcing component manufacturers to move away from Co based compositions [9]. Cr_3C_2–NiCr coatings could be a suitable substitute to WC-Co coatings, as they demonstrate comparable wear performance under erosive, cavitation, abrasive and sliding wear test conditions [8,10]. Furthermore, it has been shown that Cr_3C_2–NiCr coatings with minimal microstructural defects such as pores and cracks have excellent wear resistance [8,10].

Thermal spray is often employed to deposit coatings that combat wear and corrosion because the deposition rates are relatively fast and a larger surface area can be coated relatively easily [1]. Among the existing thermal spray processes, atmospheric plasma spray (APS) is used to deposit ceramics such as alumina, chromia based coatings to improve wear resistance [11–13] whereas, high velocity oxy fuel (HVOF) and high velocity air fuel (HVAF) are used to deposit metallic and cermet coatings such as WC-CoCr, Cr_3C_2–NiCr etc. [14–17]. The processing conditions for HVAF and HVOF differ, with the former involving a relatively lower particle temperature but a higher particle velocity [18]. It was shown that Cr_3C_2–NiCr coatings deposited by HVAF process possess excellent wear resistance compared to HVOF sprayed Cr_3C_2–NiCr coatings due to minimal microstructural defects such as porosity in the HVAF coatings [8,10]. Furthermore, Cr_3C_2 based coatings are sensitive to processing temperature as they are prone to inflight decarburization [19]. Therefore, the HVAF process can minimize the extent of decarburization in Cr_3C_2–NiCr coatings and lead to dense, superior wear resistant coatings.

GNP have attracted attention of the scientific community worldwide, partly because of their exceptional mechanical properties such as high young's modulus (up to 1 TPa) [20] and excellent tensile strength (up to 130 GPa) [21]. GNP can comprise up to 20 layers of graphene and behave in a manner similar to a single layer of graphene [22]. Furthermore, the lower manufacturing costs of GNP as compared to graphene [23], make GNP's an attractive reinforcing materials to achieve performance related benefits, as expected with graphene, in wide variety of bulk materials and coatings [24–26]. However, the use of thermal spray process for producing GNP incorporated coatings presents challenges due to low density of the GNP (problems with injection of the feedstock material) and its tendency to oxidize at low temperatures (problems with the GNP retention).

In the above context, GNP injection in the form of a suspension could serve two purposes: provide adequate momentum to the GNP-containing droplet and minimize GNP oxidation as the solvent can not only envelope the GNP but also consume a significant part of the thermal energy. So far, limited number of studies have been reported on GNP incorporated thermally sprayed coatings. Murray et al. employed suspension-HVOF (SHVOF) process to deposit GNP incorporated alumina coatings and reported ultra-low coefficient of friction, which aided in improving the wear performance [27]. Additionally, Venturi et al. deposited GNP on steel substrates using SHVOF process by radial injection and reported extremely low coefficient of friction (CoF) [28]. It has been speculated by the authors that the reason for opting radial injection of GNP over axial injection was to avoid the GNP exposure to the high thermal energy plume, which is experienced during axial injection. However, Ganvir et al. utilized suspension plasma spray (SPS), which has a higher processing temperature than SHVOF, and demonstrated its capability in retaining GNP (in YSZ matrix) via axial injection [29]. Furthermore, an innovative 'hybrid' powder – liquid feedstock combination has been previously shown to deposit coatings yielding superior performance, including exceptional wear resistance [30–34].

So far, to the best of the authors' knowledge, GNP-incorporated coatings deposited by the HVAF process have not yet been explored. Moreover, injection of a suspension in a HVAF torch is also a novelty. In this work, a hybrid approach was considered, where Cr_3C_2–NiCr in powder form and GNP as a suspension were injected coaxially to deposit GNP incorporated coatings by HVAF process. The motivation to opt for HVAF process was to utilize its capability to deposit coatings with minimal defects whereas GNP were chosen as a reinforcement to exploit their excellent mechanical properties for imparting wear resistance. Furthermore, for comparison, Cr_3C_2–NiCr coating without GNP was deposited by HVAF process using identical spray parameters. Detailed characterization of the deposited coatings was performed using SEM/EDS, XRD analyses and micro-indentation tests. Dry sliding wear tests (ball-on-disc) were utilized to assess the wear performance of the deposited coatings. Post wear analysis was performed using SEM/EDS and Profilometry analysis to evaluate and understand the wear performance and wear mechanisms of investigated coatings with and without incorporated GNP.

2. Experimental method

Low carbon steel substrates of disc geometry (25.4 mm diameter x 6 mm thick) were grit blasted with alumina of 220 grit size in order to obtain a surface roughness of approximately 3 μm (R_a). A commercially available (Amperit 588.059) chromium carbide-nickel chrome 75-25 (Cr_3C_2–NiCr) powder with a D_{50} of 18–24 μm and D_{90} of 30–40 μm, produced by Höganäs Germany GmbH, Germany, was utilized. An experimental, water-based suspension with a solid load content of 10wt. % GNP, was obtained from 2D Fab AB, Sweden. The GNP were approximately 50 μm in length. Prior to spraying, the GNP suspension was placed on rollers overnight to obtain uniform GNP dispersion. An M3™ HVAF spray gun (UniqueCoat; Richmond, USA) was used to deposit all the coatings produced in this work. For processing of the hybrid coatings, Cr_3C_2–NiCr powder and GNP suspension were simultaneously injected (co-axial injection). A schematic of the hybrid powder-suspension injection system developed in the author's lab is shown in Fig. 1.

Two variants of hybrid coatings were produced, which will be hereafter referred to as 'G1' and 'G2' whereas the standard reference Cr_3C_2–NiCr coating without graphene will be refereed as 'Cr_3C_2–NiCr-reference'. The rationale for G1 and G2 spray settings was to incorporate graphene in varying amounts during Hybrid spraying and evaluate the feasibility to retain graphene in the coating. The spray parameters used

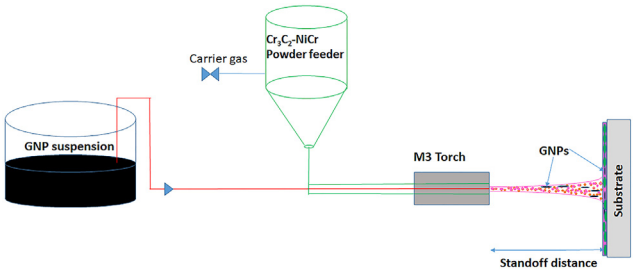

Fig. 1 – Illustration of the Powder-Suspension 'Hybrid' feedstock injection to produce GNP incorporated coatings.

to deposit the reference-Cr_3C_2–NiCr, G1 and G2 coatings are reported in Table 1.

As seen from the table, the spray parameters used for depositing G1 and Cr_3C_2–NiCr-reference coating are similar, except for co-injection of the GNP suspension. The starting GNP content injected while processing the G1 coating was approximately 3 wt.% of the total solid feedstock. In case of G1 and G2, the GNP suspension feed rate was kept the same whereas the Cr_3C_2–NiCr powder feed rate was reduced by a factor of two in order to alter the GNP content in the deposited coatings. The starting GNP feedstock content utilized in processing G2 coating corresponded to approximately 6 wt.% of the total solid feedstock. The GNP wt.% in each hybrid coating was calculated based on the ratio of solid load in the suspension and powder feed rates.

The as-deposited coatings were sectioned, mounted and polished using standard metallographic procedure discussed elsewhere [35]. The polished cross-sections were gold sputtered and analyzed by SEM (TM 3000, Hitachi, Japan). Energy Dispersive X-ray Spectroscopy (EDS) analysis on the polished surface of the coatings was performed using a Leo 1550 Gemini SEM (SEM, Oberkochen, Germany) and a Zeiss Gemini SEM 450 (Zeiss, Oberkochen, Germany). Porosity measurements were made by image analysis technique using the open domain 'ImageJ' software [36]. Fifteen cross sectional SEM micrographs at high magnification (2000 x) were considered and mean values and standard deviation of the respective porosity are reported. Hardness tests were performed on the polished cross sections using Vickers Hardness tests (SHIMADZU Corp., Japan). Fifteen independent measurements were obtained on each coating's polished cross section using 30.59 gf load and a dwell time of 15 s. A higher normal load (3059 gf) was used to generate radial cracks at the indent vertices for fracture toughness measurement, which was determined using Equation (1) [37,38].

$$A = 0.079\left(\frac{P}{a^{1.5}}\right)\log(4.5a/c) \quad (1)$$

where 'P' denotes normal load, 'c' denotes average crack length and 'a' denotes average half diagonal length of the indent.

Analysis by X-rays diffraction (XRD) was performed on the feedstock powder and on the as-sprayed coatings using a Bruker AXS D8 advance diffractometer with Cr Kα radiation (λ = 2.28970 Å).

Ball-on-disc (BoD) configuration (TRB^3 tribometer, Anton Paar, Netherlands) was used to evaluate the dry sliding wear behavior of the deposited coatings according to ASTM G99 standard at room temperature. Alumina balls (ST instruments, Netherlands) of 6 mm diameter were used as the counter material. Prior to the test, the coated specimens were polished to a surface roughness of 0.2 Ra (μm) using manual polishing and ultrasonically cleaned with acetone. A normal load of 15 N was applied for a sliding distance of 2500 m. The linear velocity was kept at 20 cm/s. Humidity within the test chamber was monitored using sensors throughout the duration of the test. Three tests were conducted for each coating variant and the lowest CoF vs. sliding time is reported. Volume loss from the worn coating was measured using white light interferometry (Profilm 3D, Filmetrics, Germany). Specific wear rates of the investigated coatings were calculated according to Equation. 2 [8].

$$\text{Spec.wear rate} = \frac{\text{Volume loss } (mm^3)}{\text{Load (N)*Sliding distance (m)}} \quad (2)$$

The worn coating surface, the wear debris and the worn alumina ball were analyzed by SEM/EDS and profilometry analysis.

3. Results and discussion

3.1. Microstructural analysis

The morphologies of the starting materials used in the present study are shown in Fig. 2. The surface SEM micrograph of the Cr_3C_2–NiCr powder showed a cluster-like appearance, typical of an agglomerated and sintered powder, according to Fig. 2(a). The particle size was predominantly observed to be approximately in the 20–30 μm range. In contrast, the SEM micrograph of GNP showed a flake-like appearance whose length was quite variable (30–70 μm range), according to Fig. 2(b). Furthermore, GNP were devoid of agglomeration, which is desirable to exploit the merits of GNP in the form of a reinforcement as agglomeration could lead to uneven distribution of GNP in the microstructure.

The cross-sectional SEM micrograph of reference Cr_3C_2–NiCr coating at lower magnification showed a delamination-

Table 1 – Spray parameters used to deposit reference Cr_3C_2–NiCr and hybrid coatings (G1 and G2).

Coating ID	Air (psi)	Fuel 1 (psi)	Fuel 2 (psi)	Carrier gas (l/min)	Powder feed rate g/min	Suspension feed rate ml/min	Standoff distance (mm)
Reference Cr_3C_2–NiCr	111	100	105	60	150	0	350
G1	111	100	105	60	150	45	350
G2	111	100	105	60	75	45	350

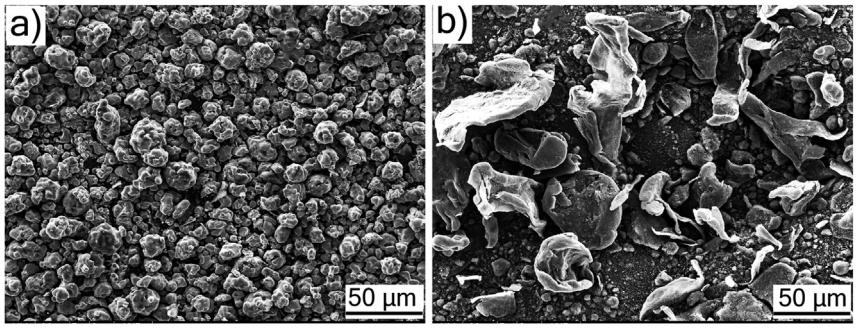

Fig. 2 – Surface SEM micrograph (SEI mode) of a) Cr3C2–NiCr powder b) Graphene Nano Platelets.

free interface with the steel substrate, according to Fig. 3(a). The bulk of coating showed minimal defects such as pores and cracks. However, a horizontal crack running through the coating close to the surface (less than 5 μm from the top) was visible. While some artefacts associated with specimen preparation cannot be ruled out, a plausible explanation for such cracks close to the coating surface could also be the lack of peening effect on the last spray pass. For wear applications, it is desirable that the coating should be devoid of cracks and other microstructural defects. Polishing of coating surface prior to wear testing eliminates such near surface defects. The coating thickness was measured to be 280 ± 10 μm. Higher magnification SEM micrograph of the cross section in Fig. 3(b) showed the harder carbide phase (gray appearance) surrounded by the binder phase (bright). Furthermore, dark regions, which could be pores or pullouts, can be seen in the SEM micrograph. The surface morphology of Cr_3C_2–NiCr coating in Fig. 3(c) showed absence of rounded particles, indicating minimal unmelts in the deposited coating microstructure.

In the case of G1 coating, a defect-free interface with the substrate was observed in the cross-sectional SEM micrograph at lower magnification, see Fig. 4(a). Furthermore, delamination crack close to the surface was observed. Thickness of G1 coating was measured to be 200 ± 10 μm. It should be mentioned that fewer number of spray passes compared to reference Cr_3C_2–NiCr coating were employed to deposit G1 coating. At higher magnification, the well-distributed carbide phase (gray) and the binder phase (white) were clearly visible, according to Fig. 4(b). However, GNP was difficult to identify from the high magnification cross sectional SEM micrograph. A probable reason could be due to their orientation in the deposited coating, since the GNP are usually extremely thin. Surface morphology of the G1 coatings showed minimal unmelts, but was also characterized by the presence of dark, island like features, as observed in Fig. 4(c). Higher magnification SEM micrograph of the dark phase revealed its dimensions to be approximately 30 μm in length, according to Fig. 4(d). The island-like, dark phase noted in the top view microstructure could be GNP as it matches the GNP dimensions.

G2 coating also showed a dense microstructure with low porosity and minimal cracks in the bulk of coating, along with delamination crack close to the surface, according to low magnification cross sectional SEM micrograph in Fig. 5(a). Thickness of the G2 coating was 180 ± 10 μm. Cross sectional SEM micrograph at higher magnification showed well-distributed carbide phase and the binder phase, according to Fig. 5(b). However, GNP was difficult to identify from the higher magnification cross sectional SEM micrographs. Surface morphology of the G2 coating at lower magnification showed minimal unmelts along with a dark phase embedded in the coating, according to Fig. 5(c). As in case of G1, a closer examination of the dark phase at higher magnification showed flake-like appearance suggestive of GNP presence, as observed in Fig. 5(d).

The porosity content in all the investigated coatings was comparable and measured to be <3%, which is desirable for mitigating wear and corrosion. To confirm that the dark phases observed in both coatings are GNP derived, SEM/EDS analyses were performed on the polished surface of the G1 coating and the results are shown in Fig. 6. The back scattered electron image in Fig. 6(a-b) clearly reveal the presence of thin flat flakes on the Cr_3C_2–NiCr matrix. The EDS maps (see Figure. 6c) acquired from the area highlighted in Fig. 6(b) reveal the features are Carbon-based and appear rather thin as the matrix features below are visible as well. Similar carbon features were not observed on the surface of the polished, GNP-free Cr_3C_2–NiCr reference specimen, which further confirms that the observed phase was derived from GNP.

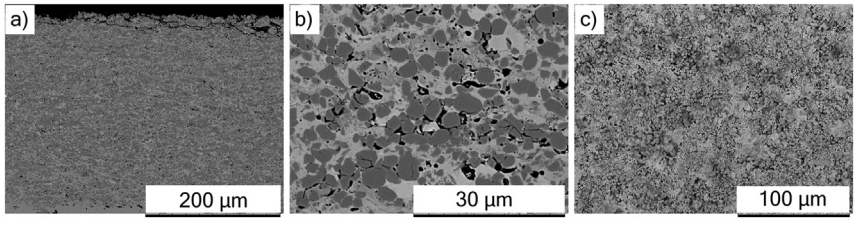

Fig. 3 – SEM analysis of the reference HVAF sprayed Cr_3C_2–NiCr reference coating a) low magnification cross section b) high magnification cross section c) surface morphology.

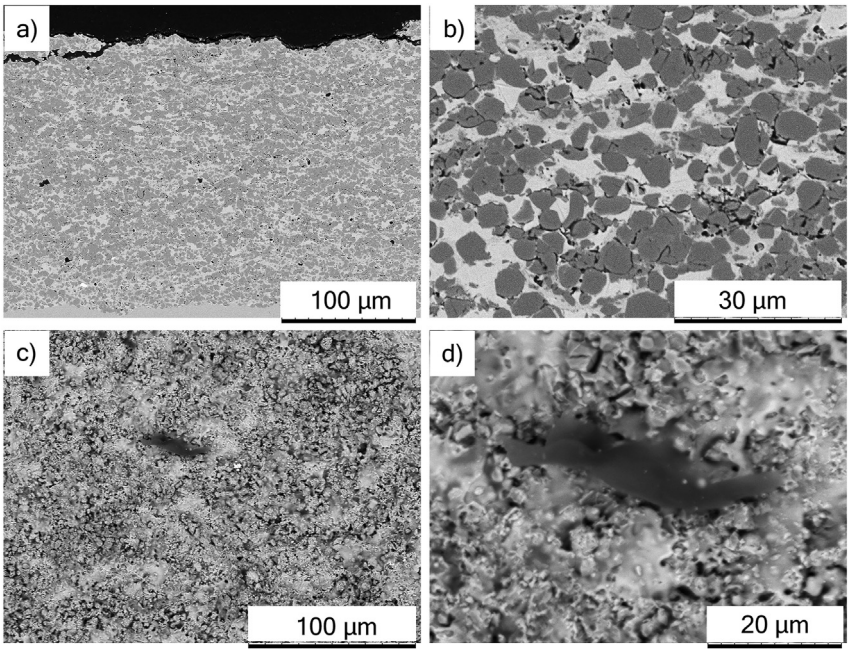

Fig. 4 – SEM analysis of the HVAF sprayed G1 (Hybrid) coating a) low magnification cross section b) high magnification cross section c) low magnification surface morphology d) high magnification surface morphology showing GNP-like appearance.

Raman measurements were performed to analyze the physical state of GNP within the sprayed coatings. However, due to the high amount of carbon in the Cr_3C_2–NiCr matrix, Raman analysis was not found to be effective in differentiating the presence of GNPs in the carbon-rich matrix on account of superposition in the acquired Raman spectra of the graphene bands on those of the carbides (Cr_3C_2–NiCr). In order to be able to distinguish the GNPs from the carbon-containing Cr_3C_2–NiCr matrix, functionalized GNPs will be investigated in a forthcoming work.

Based on the top view and cross-sectional SEM analysis, the reference Cr_3C_2–NiCr and the two ostensibly GNP-incorporated coatings bear microstructures that show similarities in terms of coating integrity, defects etc. However, the only difference is the presence of carbon-rich dark phase derived from GNP, in the case of G1 and G2 coatings, according

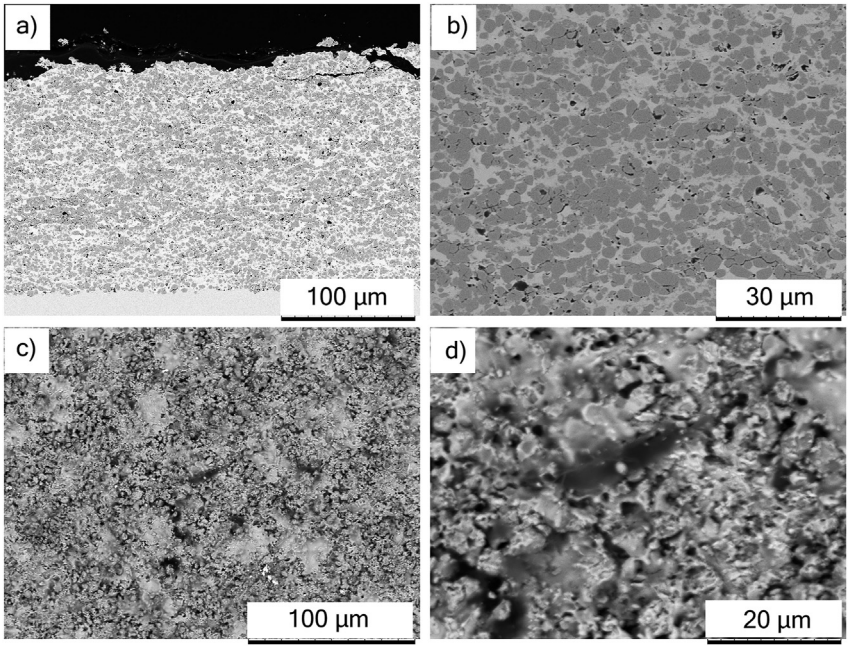

Fig. 5 – SEM analysis of the HVAF sprayed G2 (Hybrid) coating a) low magnification cross section b) high magnification cross section c) low magnification surface morphology d) high magnification surface morphology showing GNP-like appearance.

to top view SEM micrographs, which does not apparently seem to compromise the splat cohesion as the bulk of the coating was devoid of cracks. Furthermore, the G1 and G2 coatings also showed similar microstructural features (minimal unmelts, low content of defects such as pores etc.), although they were deposited using different powder-suspension feed rate ratios (higher GNP wt. % and lower overall injected solids for G2 than G1).

3.2. XRD

XRD analysis of the Cr_3C_2–NiCr feedstock powder and as-sprayed coatings are shown in Fig. 7. In the feedstock powder and as-sprayed coatings, two distinct crystalline phases, i.e. Cr_3C_2 phase and Ni-based metallic phase, were detected. However, in the as-sprayed coatings, the XRD peaks appear broader when compared to the peaks acquired from the feedstock powder. Such broadening in the peaks can be attributed to amorphization and/or grain refinement of the phases upon spraying [39,40]. Previous studies on HVAF sprayed Cr_3C_2–NiCr coatings suggests that the amorphization of the metallic matrix can be attributed to the rapid solidification occurring after spraying [41,42] or due to severe plastic deformation when the particles are colliding with the substrate [43]. The peaks broadening of the Ni(Cr) phase is clearly visible in the case of reference Cr_3C_2–NiCr and G2 coatings. In fact, the X-ray peak of the (111) crystallographic plane of the Ni(Cr) phase indexed at around 68 in X-ray spectrum of the feedstock powder, appear broad and with a strongly reduced intensity in X-ray spectrum of the reference Cr_3C_2–NiCr and G2 samples, see Fig. 7. In the X-ray spectrum acquired from the G1 sample, the (111) peak of Ni(Cr) phase had highest intensity, suggesting that the crystallinity of the Ni(Cr) metallic matrix of the G1 sample was higher compared to the sprayed reference Cr_3C_2–NiCr and G2 coatings. These findings suggest

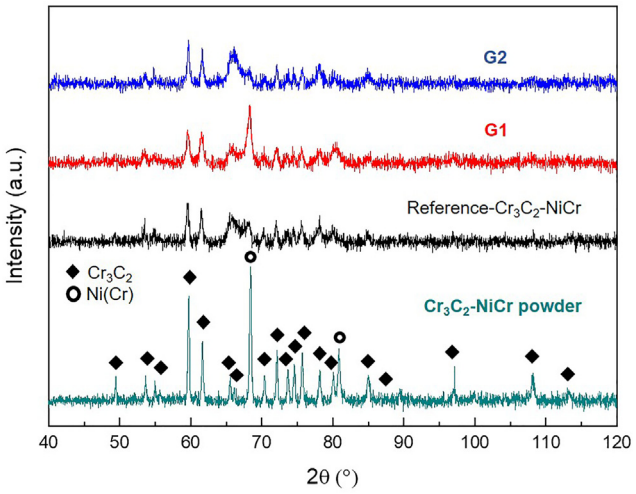

Fig. 7 – XRD analysis of the Cr_3C_2–NiCr feedstock, Cr_3C_2–NiCr reference coating, G1 coating and G2 coating.

that the introduction of the GNP suspension upon spraying the G1 composite influences the thermal history of the NiCr–Cr_3C_2 in flight. It can be hypothesized that when spraying the G1 composite coating, the Cr_3C_2–NiCr particles are characterized with a lower in-flight particle temperature due to the introduction of the GNP suspension, as compared when spraying with a conventional HVAF process (i.e. the reference Cr_3C_2–NiCr coating). The lower in-flight particle temperature can result in a higher crystallinity of the structure of the sprayed coatings, as previously observed in the case HVOF sprayed Cr_3C_2–NiCr coatings [44]. In the case of the G2 composite the effects of the GNP suspension on the particle's thermal history is compensated by a reduced Cr_3C_2–NiCr feed rate, see Table 1. Nonetheless, the as-sprayed coatings

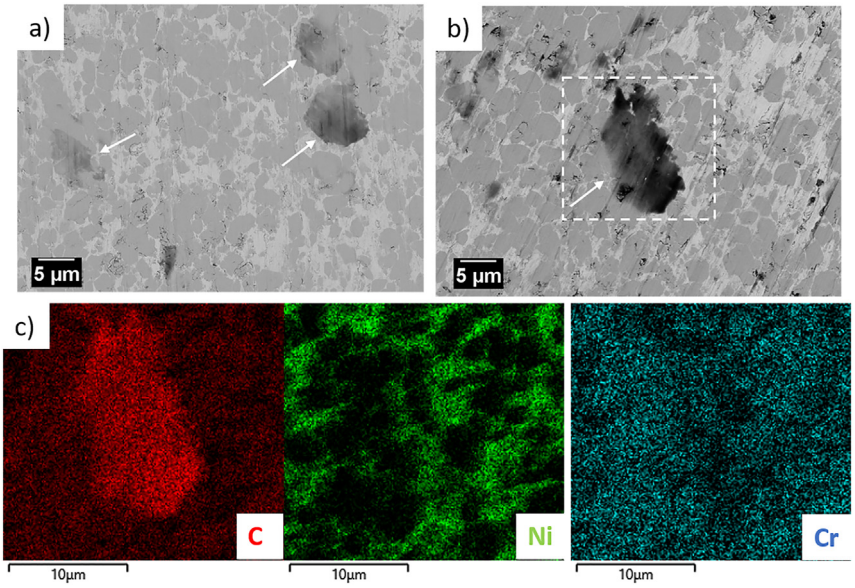

Fig. 6 – Representative SEM micrographs (BSE mode) of GNP on the polished surface of the GNP-containing coatings indicated by white arrows in a) and b). EDS maps c) showing the distribution of C, Ni and Cr in the location highlighted in b) with a white dashed box.

did not reveal any undesirable decarburization of the carbide phase and formation of new phases, which is beneficial in achieving the desired wear performance.

3.3. *Mechanical properties determined using micro-indentation*

Hardness results of deposited coatings in Fig. 8(a) show comparable hardness values for the reference Cr_3C_2–NiCr, G1 and G2 coatings. Different factors such as phase composition, coating microstructure (e.g. unmelts), porosity content, reinforcements (such as GNP content) etc. influence the coating hardness [45–49]. Although SEM analysis confirms the presence of carbon-rich phase derived from GNP in G1 and G2 coatings, the hardness appears to be similar for cermet coating with and without GNP. Furthermore, XRD analysis does not suggest any alteration of phase content in the deposited coatings with and without GNP. It could be possible that the presence of GNP in the hybrid coating are offset by the relatively poor cohesion at the GNP/Cr_3C_2–NiCr interface. As Fig. 8(b) shows, the fracture toughness measurement of the deposited coatings also shows comparable values after taking into account the measurement uncertainty. It could also be seen that the uncertainty in fracture toughness measurement was highest for the GNP containing hybrid coatings G1 and G2, suggesting inhomogeneous GNP distribution in the Cr_3C_2–NiCr matrix. Fracture toughness of the coatings investigated in this work were slightly higher than those reported by Matikanien et al. for similar coating chemistries [35]. Coatings with higher fracture toughness are desirable as they possess excellent wear resistance [50]. It should also be emphasized that the micro-indentation method estimates only the localized mechanical properties rather than the overall properties [48].

3.4. *Sliding wear test*

The coefficient of friction (CoF) vs. time plot of reference Cr_3C_2–NiCr (without GNP) is shown in Fig. 9 (a), where A, B and C represent different reference specimens tested under identical conditions. Running in stage and the steady state regime of the CoF curve can be clearly distinguished in all the tested coatings. Furthermore, the steady state CoF value for all the reference Cr_3C_2–NiCr coatings (A, B and C) were in the range of 0.3–0.4, indicating microstructural homogeneity in the reference coating. In the case of GNP incorporated hybrid coatings, G1 coating showed difference in steady state CoF values for the three test specimens (G1-A, G1-B, G1-C) where one of the G1 coatings (G1-C) had CoF values similar to the reference Cr_3C_2–NiCr coating, see Fig. 9(b). However, G1-A and G1-B coatings showed lower (approximately half) steady state CoF values than the reference coating. The lower CoF values for G1 coatings (G1-A and G1-B) could be attributed to the presence of GNP, which possess low CoF due to their self-lubricating nature. The low CoF results are in agreement with the literature where Murray et al., Venturi et al. and Derelizade et al. reported similar trend of reduction in CoF values for GNP incorporated coatings [27,51,52]. Furthermore, the difference in CoF values under identical test conditions for G1-C, as compared to G1-A and G1-B coatings, suggests inhomogeneous distribution of GNP in the microstructure. One reason for such inhomogeneous distribution of GNP can be associated to processing related challenges, where high back pressure during GNP suspension feeding resulted in pulsating nature of injection. With the absence or insignificant presence of GNP in the wear track, the coating behaves similar to the reference coating and this was evident in the case of G1-C coating. Similar scatter was observed for G2 coatings in Fig. 9(c) where G2-B coating showed lower CoF (steady state CoF of 0.2) than the G2-A and G2-C coatings (steady state CoF of approx. 0.3), indicating non-uniform distribution of GNP in the coatings. In the best-case situation, i.e. with GNP availability in the wear track, the CoF was shown to be lower (approximately half) for G2-B coating than the reference Cr_3C_2–NiCr coating. For comparison, the lowest CoF vs. time trends observed in the reference Cr_3C_2–NiCr coating, G1 and G2 coatings are shown in Fig. 10. Results demonstrate that the GNP incorporated hybrid coatings (G1 and G2) exhibit lower CoF compared to the reference hybrid coatings. Coating with low CoF can be beneficial in achieving excellent wear resistance [28]. Furthermore, for identical load conditions, the CoF values were shown to be lower in this work compared to the HVOF deposited Cr_3C_2–NiCr coatings reported elsewhere [8].

Specific wear rate of the reference Cr_3C_2–NiCr coating was higher than of the GNP incorporated hybrid coatings (G1 and G2), according to Fig. 11. Among the hybrid coatings, G1 showed the lowest specific wear rate. The specific wear rate results are in agreement with the CoF results, where the coatings with lower CoF values showed lower wear rates. The uncertainty (error bars) in specific wear rate measurement of reference Cr_3C_2–NiCr coating was smaller compared to the hybrid coatings, indicating microstructural homogeneity. Furthermore, increasing the GNP to Cr_3C_2–NiCr feed rate ratio in the case of G2 does not seem to provide added benefit in further lowering the wear rate, although G2 showed higher mean hardness than G1. Similar findings were reported by Ramachandran et al. where coatings characterized by higher hardness demonstrated inferior wear resistance [53].

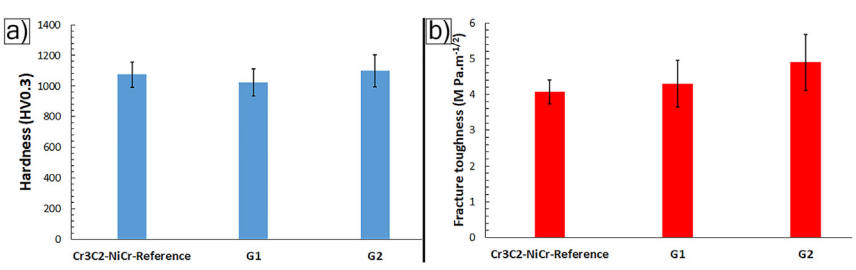

Fig. 8 – Mechanical properties of the as-deposited coatings determined using micro-indentation technique a) Hardness b) Fracture toughness.

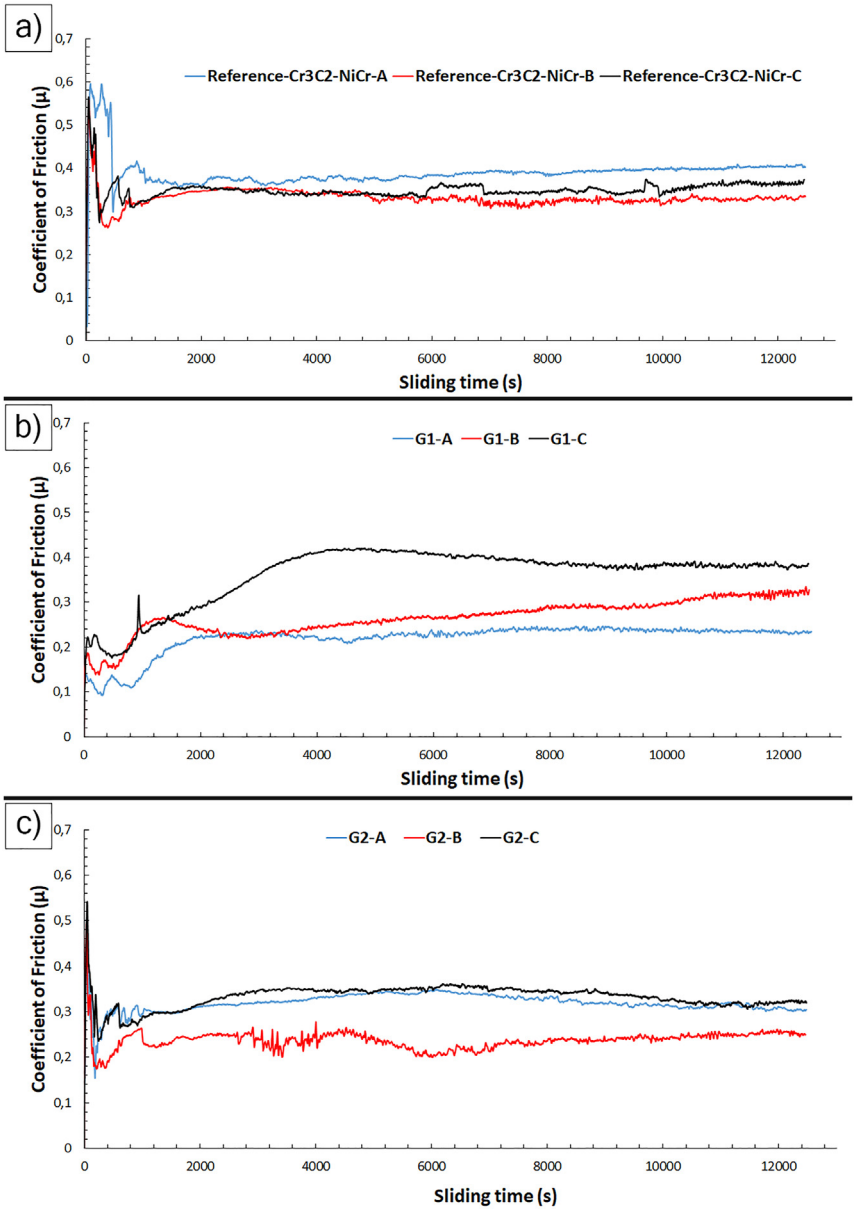

Fig. 9 – Coefficient of friction (CoF) evolution during ball-on-disc (BoD) testing of a) Cr_3C_2–NiCr reference coating b) G1 coating and c) G2 coating. A,B,C represent 3 independent BoD tests performed on each coated specimen.

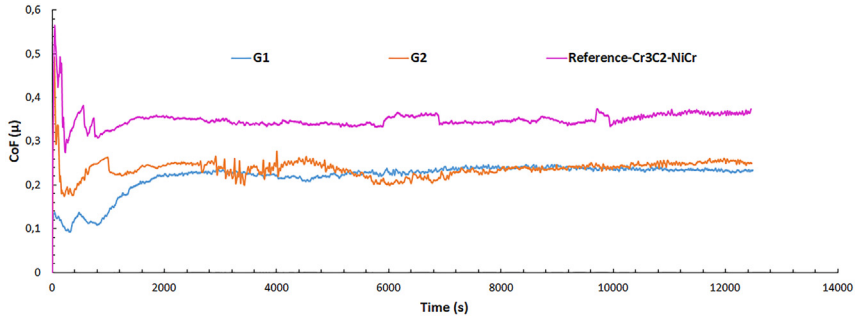

Fig. 10 – CoF comparison of the Cr_3C_2–NiCr reference coating, G1 coating and G2 coating.

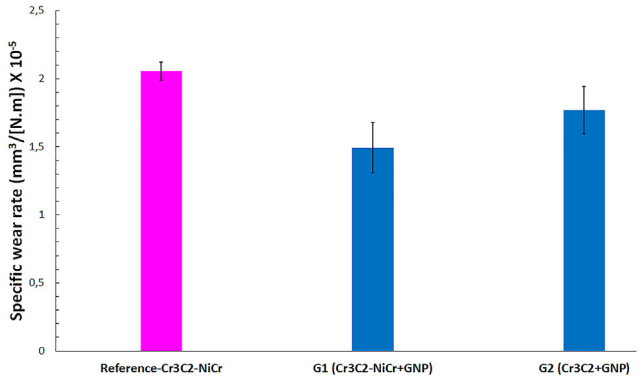

Fig. 11 – Specific wear rates of the as deposited coatings subjected to room temperature BoD tests.

Nonetheless, GNP incorporated Cr_3C_2–NiCr coatings exhibited lower wear rates and lower CoF compared to the reference coating without GNP. Post wear analysis of the investigated coatings could shed light on the wear mechanisms, which led to difference in their wear performance.

3.5. *Post- sliding wear test analysis*

Post wear SEM/EDS analysis was performed on the reference coating (relatively inferior wear performance) and G1 coating (which yielded the most superior wear performance). The surface SEM micrograph of the reference Cr_3C_2–NiCr wear track shows three distinct phases i.e. bright, grey and dark, according to Fig. 12. The bright and dark phase correspond to the chromium carbide and binder phases, which were also identified in the as-sprayed coating cross sectional microstructure of the reference Cr_3C_2–NiCr coating. The elemental maps reveal the presence of oxygen and chromium in the dark regions, indicating the tribo-oxidation as one of the prevailing wear mechanisms. During the ball-on-disc test, debris formed in the initial stages comprised of larger particles. Some of the larger debris escape the wear track whereas some remain trapped. As test progresses, the trapped debris get finer. The finer debris oxidize as a result of thermal energy generated due to friction between the two mating surfaces (alumina ball and coating surface). The oxidized debris are eventually smeared on the coating surface. Such tribo-oxide formation was shown to be beneficial in lowering the coefficient of friction and wear rate [54]. However, the capability of tribo-oxides to improve wear performance depends on several important factors such as the adhesive strength of the tribo-oxide film with the coating surface, its composition, test conditions etc. Similar findings were also reported for ball-on-disc tested Cr_3C_2–NiCr coatings in a prior study where tribo-oxidation was one of the dominant wear mechanisms [8]. Additionally, the wear debris trapped within the wear track led to micro-cracking of the harder Cr_3C_2 phase and microcutting of the ductile NiCr phase, according to Fig. 12(b), indicating the predominance of abrasive wear mechanism. Some regions of brittle fracture in the coating, leading to carbide pullout could also be seen in Fig. 12(c).

The post-test debris showed fine and larger particles, according to the SEM micrograph in Fig. 13. Elemental maps of the debris confirmed well distributed Cr, Ni and Al, indicating the material loss from both the coating surface and the ball surface. The mating alumina ball surface was also examined at the conclusion of each test. The unusual ball scar shape comprises of a circular scar apparently superimposed on an elliptical shaped scar, according to the SEM micrograph shown in Fig. 14(a). The major axis length of the elliptical scar was approximately 1 mm. It seems that the scar had a circular shape at the initial stages of the test, which later evolved into an elliptical one with test progression. The elliptical shape of the ball wear scar could be attributed to the accumulation of wear debris in the vicinity of the surfaces in contact i.e. alumina ball and the coated specimen.

The SEM micrograph of the worn G1 coating surface at low magnification in Fig. 15 (a) shows a well-distinguished wear track. Closer examination of the wear scar in Fig. 15(b) shows similarities with the reference Cr_3C_2–NiCr where bright, grey and dark phases were noted. However, the dark phase on the worn G1 coating surface appears to be elongated compared to the rounded dark phase observed in worn reference Cr_3C_2–NiCr coating. Elemental maps confirm the presence of 'O', 'C', 'Cr' and 'Ni', which suggest the presence of tribo-oxidation as one of the wear mechanism. It seems that the dark phase ('carbon'-rich phase) accommodated the in-situ formed tribo-oxides (oxides of chromium). Furthermore, abrasive wear and brittle coating fracture in Fig. 15(b) coating indicate similar wear mechanisms (tribo-oxidation, abrasive wear, brittle fracture) operating in G1 and reference Cr_3C_2–NiCr coatings.

The post wear debris of G1 coating comprised both large and fine particles, according to SEM micrograph shown in Fig. 16. Elemental maps confirmed the presence of 'Ni', 'Cr' and 'Al', indicating material loss from the coating and alumina ball surface. Furthermore, the debris from alumina ball for G1 tested coating was relatively large, in contrast to the debris collected from reference Cr_3C_2–NiCr coating that showed relatively finer alumina particles. The relatively larger size alumina debris collected in the case of G1 coating could have been thrown out of the wear track during the initial stages of test, instead of being trapped between the contact surfaces. The alumina ball used as a counter material for G1 coating showed an elliptical shape wear scar, whose major axis was approximately 600 μm, according to Fig. 14(b). The ball wear scar for G1 coating was smaller in dimension compared to the reference Cr_3C_2–NiCr coatings.

The reference and hybrid coatings showed comparable microstructural defects (porosity content) and mechanical properties, indicating that the incorporation of GNP did not compromise the microstructural integrity of hybrid coatings. Furthermore, with comparable mechanical properties and defects, the evident differences in wear behavior of conventional and hybrid coatings can be primarily attributed to the presence of GNP in hybrid coatings. Although the wear

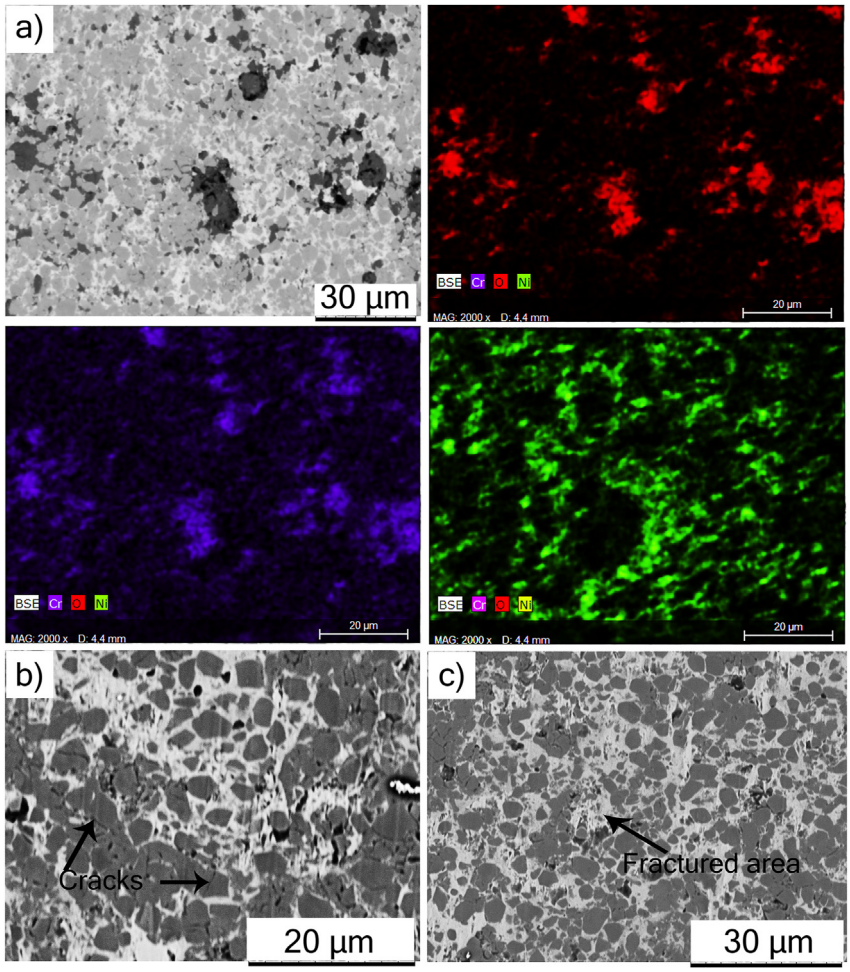

Fig. 12 – Top surface SEM micrographs (BSE mode) of worn Cr_3C_2–NiCr reference coating showing a) tribo-oxidation and its corresponding EDS analysis b) Abrasive grooving c) brittle fracture.

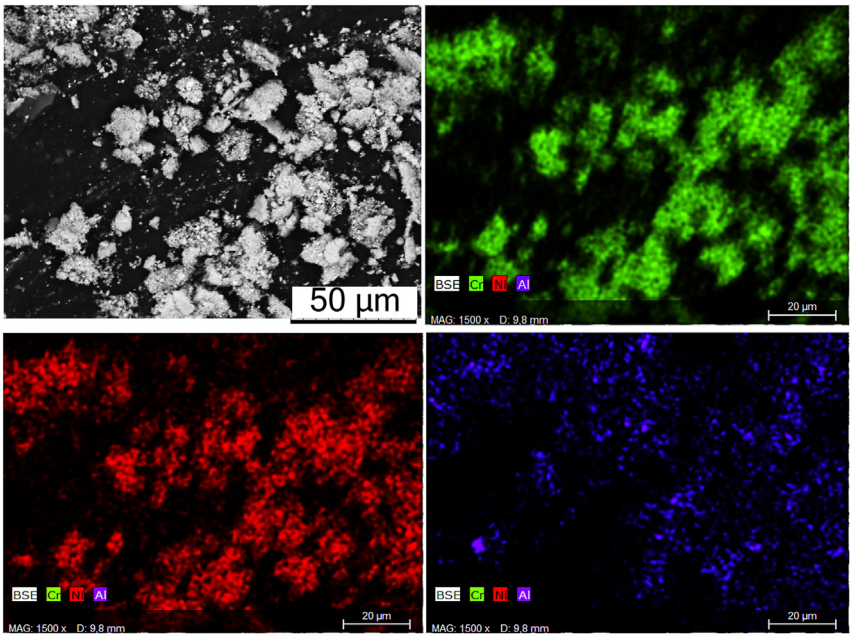

Fig. 13 – SEM/EDS analysis of the wear debris obtained from the Cr_3C_2–NiCr reference coating.

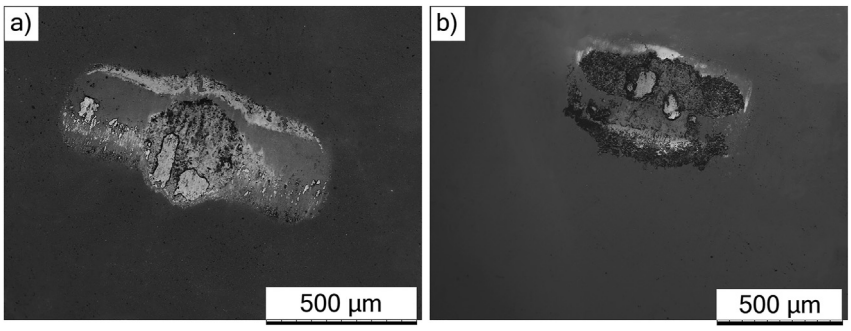

Fig. 14 – SEM micrographs (BSE mode) of the alumina ball wear scar for a) Cr_3C_2–NiCr reference coating b) G1 hybrid coating.

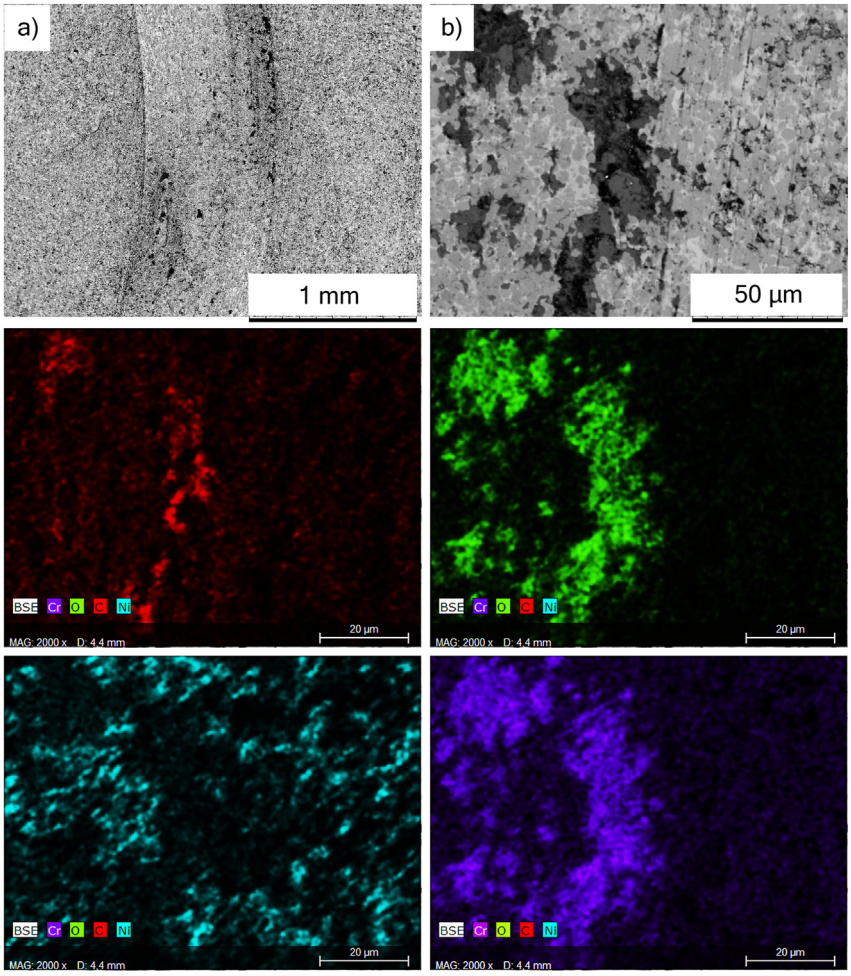

Fig. 15 – Top surface SEM analysis of worn G1 coating showing a) low magnification SEM micrograph of wear track b) high magnification SEM micrograph and its corresponding elemental maps.

mechanisms in Cr_3C_2–NiCr coatings with GNP (G1) and without GNP (reference) were similar i.e. tribo-oxidation, micro-cutting of the ductile phase and micro-cracking of the harder carbide phase, brittle fracture of the carbide etc., the additional smearing of tribo-oxides (oxides of chromium) on the carbon-rich phase derived from GNP in G1 coating could have led to lower CoF and lower specific wear rates for G1 coating compared to reference Cr_3C_2–NiCr. A schematic illustration of the wear sliding mechanisms in the Cr_3C_2–NiCr coating with and without GNP is shown in Fig. 17 where the carbon-rich phase in G1 coating acts as the accumulation site for the tribo-oxides. The improved wear resistance of G1 coating was also evident from the relatively smaller alumina ball wear scar length. Furthermore, the stable (no spike) CoF

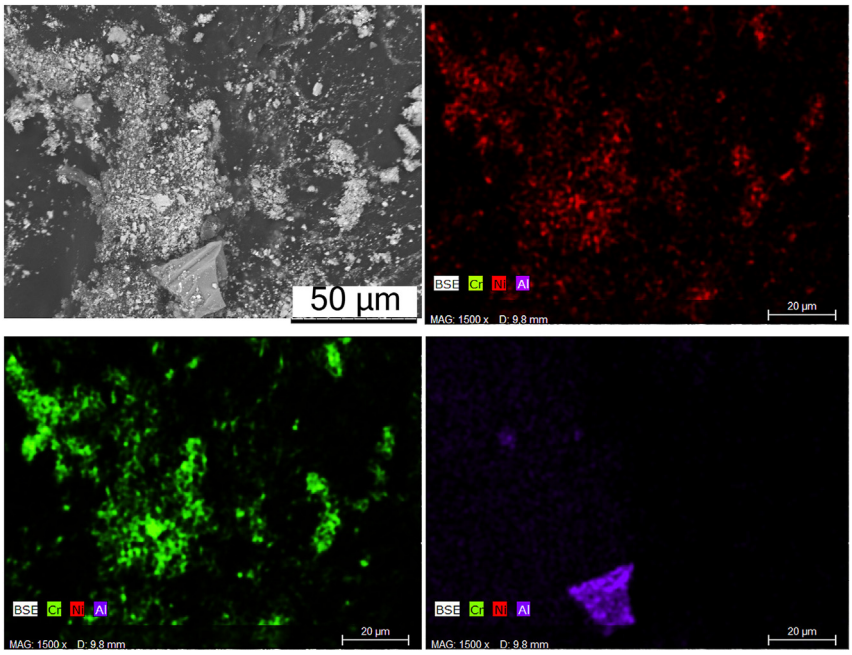

Fig. 16 – SEM/EDS analysis of wear debris collected after BoD testing of G1 hybrid coating.

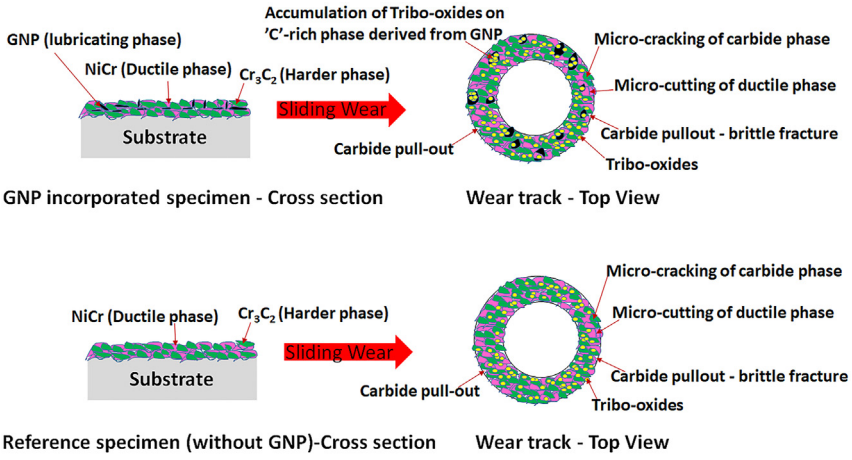

Fig. 17 – Schematic illustration of the dry sliding wear mechanisms in HVAF sprayed Cr_3C_2–NiCr coating a) with GNP b) without GNP.

values after reaching the steady state regime in all the tested coatings indicates that the in-situ formed tribo-oxides adhered well to the coating surface with progress in test time.

4. Conclusion

In this work, for the first time, a hybrid 'powder-suspension' feedstock approach was utilized to deposit GNP-incorporated Cr_3C_2–NiCr coatings (G1 and G2) by HVAF process. For comparison, a reference Cr_3C_2–NiCr coating (without graphene) was also deposited by HVAF process. SEM, XRD analysis and micro-indentation tests were used to perform detailed characterization the HVAF deposited Cr_3C_2–NiCr coatings (with and without GNP). Dry sliding wear test conditions were used to evaluate the wear behavior of the deposited coatings. Post wear analysis was performed using SEM/EDS and profilometry analysis to gain further insights. It was shown that:

- Suspension injection in HVAF process is a facile approach to incorporate GNP in a powder-derived wear coating using a hybrid approach.
- SEM analysis of the GNP incorporated coatings (G1 and G2) and the reference Cr_3C_2–NiCr coating had similar microstructures, in terms of coating integrity, minimal unmelts and defects.

- SEM/EDS analyses of the GNP incorporated coatings confirmed the presence of carbon-rich, GNP derived phase in the as-sprayed coatings.
- XRD analysis of the feedstock and as-deposited coatings showed the presence of two crystalline phases: Cr_2C_3 and Ni(Cr). Furthermore, no decarburization of the carbide was observed in all the HVAF sprayed coatings.
- The coefficient of friction and specific wear rates were lower for GNP incorporated G1, G2 coatings compared to the reference Cr_3C_2–NiCr coating.
- Wear mechanisms for GNP incorporated and reference coatings were similar, where tribo-oxidation, abrasive wear and brittle fracture were predominant in the tested coatings. Furthermore, debris analysis showed material loss from the coating and ball surface for coatings with and without GNP. However, the ball scar dimensions and the debris particle size differed in the tested coatings.

This work amply demonstrated that carbon-rich phase derived from GNP can be retained in the HVAF sprayed coatings using powder-suspension 'hybrid' feedstock injection route. Although its quantification in the deposited coatings still remains a challenge, the benefits of GNP incorporated coatings in terms of wear performance (lower coefficient of friction, lower specific wear rates) are clearly evident and, at the same time encouraging to develop superior wear-resistant coatings. Furthermore, homogeneous GNP distribution was an issue in the current study as the fracture toughness and CoF values for hybrid coatings varied during test repetitions compared to the reference coating. Addressing the processing related challenges i.e. the pulsating nature of suspension injection due to high back pressure, can help to overcome the inhomogeneous distribution of GNP. Additionally, utilizing finer GNP feedstock (<5 μm length) in the form of suspension could be beneficial in achieving homogenous distribution of GNP in the deposited coating, which could further enhance the wear performance.

Declaration of Competing Interest

The authors declare that they have no known competing financial interests or personal relationships that could have appeared to influence the work reported in this paper.

Acknowledgements

The project is financed by the national Strategic Innovation Programme for graphene, SIO Grafen, supporting the industrial graphene development in Sweden. The programme is supported by the Swedish government agencies Vinnova (Sweden's Innovation Agency), the Swedish Energy Agency and the Swedish Research Council Formas. The project grant nr. is Dnr 2018–03315. The authors acknowledge the help from Mr. Sven Forsberg from 2D Fab, AB, Sweden for providing the GNP suspension. The authors also thank Mr. Magnus Sandberg, University West, for assisting in spraying the coatings.

REFERENCES

[1] Tejero-Martin D, Rezvani Rad M, McDonald A, Hussain T. Beyond traditional coatings: a review on thermal-sprayed functional and smart coatings. J Therm Spray Technol Apr. 2019;28(4):598–644. https://doi.org/10.1007/s11666-019-00857-1.

[2] Aranke O, Algenaid W, Awe S, Joshi S. Coatings for automotive gray cast iron brake discs: a review. Coatings Sep. 2019;9(9):552. https://doi.org/10.3390/coatings9090552.

[3] He J, Schoenung JM. A review on nanostructured WC–Co coatings. Surf Coating Technol Aug. 2002;157(1):72–9. https://doi.org/10.1016/S0257-8972(02)00141-X.

[4] Hoornaert T, Hua ZK, Zhang JH. Hard wear-resistant coatings: a review. In: Advanced tribology; 2010. p. 774–9.

[5] Berghaus JO, Marple B, Moreau C. Suspension plasma spraying of nanostructured WC-12Co coatings. J Therm Spray Technol Dec. 2006;15(4):676–81. https://doi.org/10.1361/105996306X147072.

[6] Berget J, Rogne T, Bardal E. Erosion–corrosion properties of different WC–Co–Cr coatings deposited by the HVOF process—influence of metallic matrix composition and spray powder size distribution. Surf Coating Technol Jun. 2007;201(18):7619–25. https://doi.org/10.1016/j.surfcoat.2007.02.032.

[7] De Boeck M, Kirsch-Volders M, Lison D. Cobalt and antimony: genotoxicity and carcinogenicity. Mutat Res Mol Mech Mutagen Dec. 2003;533(1):135–52. https://doi.org/10.1016/j.mrfmmm.2003.07.012.

[8] Matikainen V, Bolelli G, Koivuluoto H, Sassatelli P, Lusvarghi L, Vuoristo P. Sliding wear behaviour of HVOF and HVAF sprayed Cr3C2-based coatings. Wear Oct. 2017;388–389:57–71. https://doi.org/10.1016/j.wear.2017.04.001.

[9] Jensen AA, Tüchsen F. Cobalt exposure and cancer risk. Crit Rev Toxicol 1990;20(6):427–37. https://doi.org/10.3109/10408449009029330.

[10] Matikainen V, Koivuluoto H, Vuoristo P. A study of Cr3C2-based HVOF- and HVAF-sprayed coatings: abrasion, dry particle erosion and cavitation erosion resistance. Wear Apr. 2020;446–447:203188. https://doi.org/10.1016/j.wear.2020.203188.

[11] Abdel-Samad AA, El-Bahloul AMM, Lugscheider E, Rassoul SA. A comparative study on thermally sprayed alumina based ceramic coatings. J Mater Sci Jun. 2000;35(12):3127–30. https://doi.org/10.1023/A:1004824104162.

[12] Niemi K, Vuoristo P, Mäntylä T. Properties of alumina-based coatings deposited by plasma spray and detonation gun spray processes. J Therm Spray Technol Jun. 1994;3(2):199–203. https://doi.org/10.1007/BF02648279.

[13] Wang Bu-Qian, Shui Zheng Rong, Levy AV. Sliding wear of thermal-sprayed chromia coatings. Wear Jun. 1990;138(1):93–110. https://doi.org/10.1016/0043-1648(90)90170-F.

[14] Varis T, Suhonen T, Ghabchi A, Valarezo A, Sampath S, Liu X, et al. Formation mechanisms, structure, and properties of HVOF-sprayed WC-CoCr coatings: an approach toward process maps. J Therm Spray Technol Aug. 2014;23(6):1009–18. https://doi.org/10.1007/s11666-014-0110-5.

[15] Ahmed R, Faisal NH, Al-Anazi NM, Al-Mutairi S, Toma FL, Berger LM, et al. Structure property relationship of suspension thermally sprayed WC-Co nanocomposite coatings. J Therm Spray Technol Feb. 2015;24(3):357–77. https://doi.org/10.1007/s11666-014-0174-2.

[16] Tao K, Zhang J, Cui H, Zhou X, Zhang J. Fabrication of conventional and nanostructured NiCrC coatings via HVAF

technique. Trans Nonferrous Metals Soc China Apr. 2008;18(2):262–9. https://doi.org/10.1016/S1003-6326(08)60046-1.
[17] Zhou W, Zhou K, Li Y, Deng C, Zeng K. High temperature wear performance of HVOF-sprayed Cr3C2-WC-NiCoCrMo and Cr3C2-NiCr hardmetal coatings. Appl Surf Sci Sep. 2017;416:33–44. https://doi.org/10.1016/j.apsusc.2017.04.132.
[18] Joshi S, Nylen P. Advanced coatings by thermal spray processes. Technologies Dec. 2019;7(4):79. https://doi.org/10.3390/technologies7040079.
[19] Mahade S, Narayan K, Govindarajan S, Björklund S, Curry N, Joshi S. Exploiting suspension plasma spraying to deposit wear-resistant carbide coatings. Materials Jan. 2019;12(15):2344. https://doi.org/10.3390/ma12152344.
[20] Frank IW, Tanenbaum DM, van der Zande AM, McEuen PL. Mechanical properties of suspended graphene sheets. J Vac Sci Technol B Microelectron Nanometer Struct Process Meas Phenom. Nov. 2007;25(6):2558–61. https://doi.org/10.1116/1.2789446.
[21] Lee C, Wei X, Kysar JW, Hone J. Measurement of the elastic properties and intrinsic strength of monolayer graphene. Science Jul. 2008;321(5887):385–8. https://doi.org/10.1126/science.1157996.
[22] Nieto A, Lahiri D, Agarwal A. Synthesis and properties of bulk graphene nanoplatelets consolidated by spark plasma sintering. Carbon Sep. 2012;50(11):4068–77. https://doi.org/10.1016/j.carbon.2012.04.054.
[23] Kotov NA. Carbon sheet solutions. Nature Jul. 2006;442(7100):7100. https://doi.org/10.1038/442254a.
[24] Munir K, Wen C, Li Y. Graphene nanoplatelets-reinforced magnesium metal matrix nanocomposites with superior mechanical and corrosion performance for biomedical applications. J Magnes Alloys Mar. 2020;8(1):269–90. https://doi.org/10.1016/j.jma.2019.12.002.
[25] Bhadauria A, Singh LK, Laha T. Combined strengthening effect of nanocrystalline matrix and graphene nanoplatelet reinforcement on the mechanical properties of spark plasma sintered aluminum based nanocomposites. Mater Sci Eng, A Mar. 2019;749:14–26. https://doi.org/10.1016/j.msea.2019.02.007.
[26] Pinto AM, Gonçalves C, Sousa DM, Ferreira AR, Moreira JA, Gonçalves IC, et al. Smaller particle size and higher oxidation improves biocompatibility of graphene-based materials. Carbon Apr. 2016;99:318–29. https://doi.org/10.1016/j.carbon.2015.11.076.
[27] Murray JW, Rance GA, Xu F, Hussain T. Alumina-graphene nanocomposite coatings fabricated by suspension high velocity oxy-fuel thermal spraying for ultra-low-wear. J Eur Ceram Soc Apr. 2018;38(4):1819–28. https://doi.org/10.1016/j.jeurceramsoc.2017.10.022.
[28] Venturi F, Rance GA, Thomas J, Hussain T. A low-friction graphene nanoplatelets film from suspension high velocity oxy-fuel thermal spray. AIP Adv Feb. 2019;9(2):025216. https://doi.org/10.1063/1.5089021.
[29] Ganvir A, Björklund S, Yao Y, Vadali SVSS, Klement U, Joshi S. A facile approach to deposit graphenaceous composite coatings by suspension plasma spraying. Coatings Mar. 2019;9(3):3. https://doi.org/10.3390/coatings9030171.
[30] Murray JW, Leva A, Joshi S, Hussain T. Microstructure and wear behaviour of powder and suspension hybrid Al2O3–YSZ coatings. Ceram Int May 2018;44(7):8498–504. https://doi.org/10.1016/j.ceramint.2018.02.048.
[31] Björklund S, Goel S, Joshi S. Function-dependent coating architectures by hybrid powder-suspension plasma spraying: injector design, processing and concept validation. Mater Des Mar. 2018;142:56–65. https://doi.org/10.1016/j.matdes.2018.01.002.
[32] Sivakumar G, Banerjee S, Raja VS, Joshi SV. Hot corrosion behavior of plasma sprayed powder-solution precursor hybrid thermal barrier coatings. Surf Coating Technol Sep. 2018;349:452–61. https://doi.org/10.1016/j.surfcoat.2018.06.021.
[33] Mahade S, Baiamonte L, Sadeghimeresht E, Björklund S, Marra F, Joshi S. Novel utilization of powder-suspension hybrid feedstock in HVAF spraying to deposit improved wear and corrosion resistant coatings. Surf Coating Technol Apr. 2021;412:127015. https://doi.org/10.1016/j.surfcoat.2021.127015.
[34] Ganvir A, Goel S, Govindarajan S, Jahagirdar AR, Björklund S, Klement U, et al. Tribological performance assessment of Al2O3-YSZ composite coatings deposited by hybrid powder-suspension plasma spraying. Surf Coating Technol Mar. 2021;409:126907. https://doi.org/10.1016/j.surfcoat.2021.126907.
[35] Mahade S, Curry N, Björklund S, Markocsan N, Nylén P. Thermal conductivity and thermal cyclic fatigue of multilayered Gd2Zr2O7/YSZ thermal barrier coatings processed by suspension plasma spray. Surf Coating Technol Dec. 2015;283:329–36. https://doi.org/10.1016/j.surfcoat.2015.11.009.
[36] ImageJ," Softonic. https://imagej.en.softonic.com.
[37] Evans AG, Wilshaw TR. Quasi-static solid particle damage in brittle solids—I. Observations analysis and implications. Acta Metall Oct. 1976;24(10):939–56. https://doi.org/10.1016/0001-6160(76)90042-0.
[38] Matikainen V, Bolelli G, Koivuluoto H, Honkanen M, Vippola M, Lusvarghi L, et al. A study of Cr3C2-based HVOF- and HVAF-sprayed coatings: microstructure and carbide retention. J Therm Spray Technol Aug. 2017;26(6):1239–56. https://doi.org/10.1007/s11666-017-0578-x.
[39] Liu Q, Bai Y, Wang HD, Ma GZ, Liu M, Chu CY, et al. Microstructural evolution of carbides and its effect on tribological properties of SAPS or HVOF sprayed NiCr–Cr3C2 coatings. J Alloys Compd Sep. 2019;803:730–41. https://doi.org/10.1016/j.jallcom.2019.06.291.
[40] Qin E, Wang B, Li W, Ma W, Lu H, Wu S. Optimized microstructure and properties of Cr3C2-NiCr cermet coating by HVOF/laser hybrid processing. J Therm Spray Technol Jun. 2019;28(5):1072–80. https://doi.org/10.1007/s11666-019-00877-x.
[41] Matthews S, James B, Hyland M. The role of microstructure in the mechanism of high velocity erosion of Cr3C2–NiCr thermal spray coatings: Part 1 — as-sprayed coatings. Surf Coating Technol Jan. 2009;203(8):1086–93. https://doi.org/10.1016/j.surfcoat.2008.10.005.
[42] Matthews S, James B, Hyland M. Erosion of oxide scales formed on Cr3C2–NiCr thermal spray coatings. Corrosion Sci Nov. 2008;50(11):3087–94. https://doi.org/10.1016/j.corsci.2008.08.032.
[43] Bolelli G, Berger LM, Börner T, Koivuluoto H, Matikainen V, Lusvarghi L, et al. Sliding and abrasive wear behaviour of HVOF- and HVAF-sprayed Cr3C2–NiCr hardmetal coatings. Wear Jul. 2016;358–359:32–50. https://doi.org/10.1016/j.wear.2016.03.034.
[44] Poirier D, Legoux J-G, Lima RS. Engineering HVOF-sprayed Cr3C2-NiCr coatings: the effect of particle morphology and spraying parameters on the microstructure, properties, and high temperature wear performance. J Therm Spray Technol Mar. 2013;22(2):280–9. https://doi.org/10.1007/s11666-012-9833-3.
[45] Jia K, Fischer TE, Gallois B. Microstructure, hardness and toughness of nanostructured and conventional WC-Co composites. Nanostruct Mater Jul. 1998;10(5):875–91. https://doi.org/10.1016/S0965-9773(98)00123-8.
[46] Tao K, Zhou X, Cui H, Zhang J. Microhardness variation in heat-treated conventional and nanostructured NiCrC

coatings prepared by HVAF spraying. Surf Coating Technol Feb. 2009;203(10):1406–14. https://doi.org/10.1016/j.surfcoat.2008.11.020.

[47] Saleem A, Zhang Y, Gong H, Majeed MK, Jing J, Lin X, et al. Enhanced thermal conductivity and mechanical properties of a GNP reinforced Si3N4 composite. RSC Adv Dec. 2019;9(68):39986–92. https://doi.org/10.1039/C9RA09286B.

[48] Mahade S, Venkat A, Curry N, Leitner M, Joshi S. Erosion performance of atmospheric plasma sprayed thermal barrier coatings with diverse porosity levels. Coatings Jan. 2021;11(1):1. https://doi.org/10.3390/coatings11010086.

[49] Mahade S, Aranke O, Björklund S, Dizdar S, Awe S, Mušálek R, et al. Influence of processing conditions on the microstructure and sliding wear of a promising Fe-based coating deposited by HVAF. Surf Coating Technol Mar. 2021;409:126953. https://doi.org/10.1016/j.surfcoat.2021.126953.

[50] Sevim I, Eryurek IB. Effect of fracture toughness on abrasive wear resistance of steels. Mater Des Jan. 2006;27(10):911–9. https://doi.org/10.1016/j.matdes.2005.03.009.

[51] Venturi F, Pulsford J, Hussain T. A novel approach to incorporate graphene nanoplatelets to Cr2O3 for low-wear coatings. Mater Lett Oct. 2020;276:128283. https://doi.org/10.1016/j.matlet.2020.128283.

[52] Derelizade K, Venturi F, Wellman RG, Khlobystov A, Hussain T. Structural changes of thermal sprayed graphene nano platelets film into amorphous carbon under sliding wear. Appl Surf Sci Oct. 2020;528:146315. https://doi.org/10.1016/j.apsusc.2020.146315.

[53] Ramachandran CS, Balasubramanian V, Ananthapadmanabhan PV. Erosion of atmospheric plasma sprayed rare earth oxide coatings under air suspended corundum particles. Ceram Int Jan. 2013;39(1):649–72. https://doi.org/10.1016/j.ceramint.2012.06.077.

[54] Vashishtha N, Sapate SG, Gahlot JS, Bagde P. Effect of tribo-oxidation on friction and wear behaviour of HVOF sprayed WC–10Co–4Cr coating. Tribol Lett Mar. 2018;66(2):56. https://doi.org/10.1007/s11249-018-1006-1.